

Northumbria Research Link

Citation: Zhang, Tian, Ji, Han, Ghassemlooy, Zabih, Tang, Xuan, Lin, Bangjiang and Qiao, Shuang (2020) Spectrum-Efficient Triple-Layer Hybrid Optical OFDM for IM/DD-Based Optical Wireless Communications. IEEE Access, 8. pp. 10352-10362. ISSN 2169-3536

Published by: IEEE

URL: <https://doi.org/10.1109/ACCESS.2020.2964792>
<<https://doi.org/10.1109/ACCESS.2020.2964792>>

This version was downloaded from Northumbria Research Link: <http://nrl.northumbria.ac.uk/42178/>

Northumbria University has developed Northumbria Research Link (NRL) to enable users to access the University's research output. Copyright © and moral rights for items on NRL are retained by the individual author(s) and/or other copyright owners. Single copies of full items can be reproduced, displayed or performed, and given to third parties in any format or medium for personal research or study, educational, or not-for-profit purposes without prior permission or charge, provided the authors, title and full bibliographic details are given, as well as a hyperlink and/or URL to the original metadata page. The content must not be changed in any way. Full items must not be sold commercially in any format or medium without formal permission of the copyright holder. The full policy is available online: <http://nrl.northumbria.ac.uk/policies.html>

This document may differ from the final, published version of the research and has been made available online in accordance with publisher policies. To read and/or cite from the published version of the research, please visit the publisher's website (a subscription may be required.)



Northumbria
University
NEWCASTLE

Received December 21, 2019, accepted January 5, 2020, date of publication January 8, 2020, date of current version January 17, 2020.

Digital Object Identifier 10.1109/ACCESS.2020.2964792

Spectrum-Efficient Triple-Layer Hybrid Optical OFDM for IM/DD-Based Optical Wireless Communications

TIAN ZHANG^{1,*}, (Member, IEEE), HAN JI^{1,3,*},
ZABIH GHASSEMLOOY^{2,3}, (Senior Member, IEEE),
XUAN TANG³, BANGJIANG LIN³, AND SHUANG QIAO¹

¹School of Physics, Northeast Normal University, Changchun 130024, China

²Optical Communications Research Group, Faculty of Engineering and Environment, Northumbria University, Newcastle upon Tyne NE1 8ST, U.K.

³Quanzhou Institute of Equipment Manufacturing, Haixi Institutes, Chinese Academy of Sciences, Quanzhou 362200, China

Corresponding author: Shuang Qiao (qiaos810@163.com)

This work was supported in part by the Foundation for Excellent Young Talents of Jilin Province under Grant 20190103010JH, in part by the 13th Five-Year Science and Technology Research Project of Education Department of Jilin Province under Grant JJKH20190277KJ, in part by the Fundamental Research Funds for the Central Universities under Grant 2412018QD002, in part by the National Natural Science Foundation of China under Grant 11905028, in part by the Science and Technology Program of Quanzhou under Grant 2019C010R, in part by the International Science and Technology Cooperation Program of Fujian Province under Grant 201710020, and in part by the Scientific Research Instrument and Equipment CAS under Grant YJKYYQ20170052.

*Tian Zhang and Han Ji are co-first authors.

ABSTRACT In this paper, a triple-layer hybrid optical orthogonal frequency division multiplexing (THO-OFDM) for intensity modulation with direct detection (IM/DD) systems with a high spectral efficiency is proposed. We combine N -point asymmetrically clipped optical orthogonal frequency division multiplexing (ACO-OFDM), $N/2$ -point ACO-OFDM, and $N/2$ -point pulse amplitude modulated discrete multitone (PAM-DMT) in a single frame for simultaneous transmission. The time- and frequency-domain demodulation methods are introduced by fully exploiting the special structure of the proposed THO-OFDM. Theoretical analysis show that, the proposed THO-OFDM can reach the spectral efficiency limit of the conventional layered ACO-OFDM (LACO-OFDM). Simulation results demonstrate that, the time-domain receiver offers improved bit error rate (BER) performance compared with the frequency-domain with $\sim 40\%$ reduced computation complexity when using 512 subcarriers. Furthermore, we show a 3 dB improvement in the peak-to-average power ratio (PAPR) compared with LACO-OFDM for the same three layers.

INDEX TERMS LACO-OFDM, PAM-DMT, spectral efficiency, computation complexity, PAPR.

I. INTRODUCTION

In the last decades, the increasing requirement for mobile devices and access to high-speed networks has put additional pressure on the radio-frequency (RF) spectrum usage [1], [2]. To address this problem, optical wireless communications (OWC) including the light-emitting diodes (LEDs)-based visible light communications (VLC) has been investigated to offer high-speed data links in certain key applications [2]–[5]. Due to its advantages of huge spectrum resource, lower power consumption, higher transmission data rates R_b and the immunity to RF electromagnetic interference, VLC is seen as a promising complementary wireless technology to

the current RF in indoor (mostly), outdoor and underwater applications [6]–[11].

However, the first major issue in VLC is the low modulation bandwidth B_{mod} of commercial LEDs (< 5 MHz), which limits the transmission capacity [12], [13]. Advanced equalization techniques and spectrum-efficient modulation techniques were thereafter proposed to improve B_{mod} and therefore R_b [14]–[17]. In addition, multi-carrier modulation scheme of orthogonal frequency division multiplexing (OFDM) has been investigated to increase R_b because of their higher spectral efficiency η_{se} compared with the classical most widely used on-off keying (OOK) [18]. Since the OFDM signal needs to be both real and positive in intensity modulation with direct detection (IM/DD) optical communications, asymmetrically clipped optical

The associate editor coordinating the review of this manuscript and approving it for publication was Kezhi Wang.

OFDM (ACO-OFDM), DC-biased optical OFDM (DCO-OFDM) and pulse amplitude modulated discrete multitone (PAM-DMT) have been proposed [19], [20]. In DCO-OFDM, high DC-bias level is required to ensure a unipolar positive OFDM signal at the cost of reduced power efficiency. Although both ACO-OFDM and PAM-DMT do not need high DC-bias, η_{se} is still not fully exploited because of the lower subcarrier utilization and the one-dimension PAM mapping, respectively. Therefore, a hybrid QAM and PAM can be used to improve η_{se} [21].

To further improve η_{se} of OFDM and DMT, several spectrum-efficient schemes were proposed recently [22]–[26]. In [22] and [23], a layered optical OFDM technique was proposed for IM/DD optical systems using anti-periodic OFDM signals for simultaneous transmission. In [24], a layered ACO-OFDM (LACO-OFDM) scheme was proposed by combining L -layer ACO-OFDM signals with different effective subcarriers in the time domain (TD) to improve η_{se} of conventional ACO-OFDM. A similar method termed augmented spectral efficiency discrete multitone (ASE-DMT) was proposed to improve η_{se} of conventional PAM-DMT [25], [26]. Note that, although layered-OFDM schemes can remove the spectral efficiency gap between unipolar OFDM and DCO-OFDM, their efficiency limits will require infinite layers to superimpose, which is not possible in real applications. Moreover, the combination and distortion cancellation of too many layers in the time or frequency domain would lead to an increased system complexity (i.e., hardware implementation).

In this paper, we propose a novel spectrum-efficient triple-layer hybrid optical OFDM (THO-OFDM), which offers a trade-off between η_{se} and complexity compared with DCO-OFDM. We show that, the proposed THO-OFDM can reach η_{se} limit of LACO-OFDM using only 3-layer and including N -point ACO-OFDM, $N/2$ -point ACO-OFDM and $N/2$ -point PAM-DMT in a single TD frame. Analysis and simulation results show that, the proposed THO-OFDM outperforms conventional LACO-OFDM in terms of computation complexity and PAPR.

The remainder of this paper is organized as follows. In Section II, the conventional LACO-OFDM is briefly described, while in Section III the proposed THO-OFDM and its time/frequency-domain (FD) transceiver are described in detail. Theoretical analysis of spectral efficiency, computation complexity and BER performance are given in Section IV. Simulation results and performance comparisons of the proposed THO-OFDM are presented in Section V. Finally, conclusions are drawn in Section VI.

II. CONVENTIONAL LACO-OFDM SYSTEM

In classical ACO-OFDM, the input bits are converted into complex symbols of quadrature amplitude modulation (QAM). Following Hermitian symmetry, only the odd subcarriers are used prior to inverse fast Fourier transform (IFFT). Therefore, for ACO-OFDM the input FD vector is

given by:

$$X = [0, X_1, 0, X_3, \dots, X_{N/2-1}, 0, X_{N/2-1}^*, 0, \dots, X_3^*, 0, X_1^*], \quad (1)$$

where N is the number of subcarriers and $*$ denotes the conjugate symmetric operation. Following IFFT, the TD signal is expressed as:

$$x(n) = \frac{1}{\sqrt{N}} \sum_{k=0}^{N-1} X(k) \exp\left(j \frac{2\pi}{N} kn\right), \quad (2)$$

where $n = 0, 1, \dots, N-1$, and $x(n)$ is a bipolar signal, which satisfies the antisymmetric property given by:

$$x(n) = -x(n + N/2), \quad n = 0, 1, \dots, N/2 - 1. \quad (3)$$

The ACO-OFDM signal is obtained by a negative clipping without losing any information. Based on this feature, L -layer ($L \geq 2$) LACO-OFDM is constructed by superposition of $[N, N/2, \dots, N/2^{L-1}]$ points ACO-OFDM signals in the TD [24]. Following a redundant replication process, each layer with the same ACO-OFDM signal length are combined for simultaneous transmission. Thus, the LACO-OFDM in the TD can be defined as:

$$x_{\text{LACO}} = \sum_{l=1}^L \left[x_{\text{ACO},n}^{(l)} \right]_c, \quad n = 0, 1, \dots, N-1. \quad (4)$$

where L denotes the maximum number of layers in LACO-OFDM, $\left[x_{\text{ACO},n}^{(l)} \right]_c$ denotes the repeated ACO-OFDM signal in the l^{th} layer after redundant replication process, and $[\cdot]_c$ denotes the negative clipping operation. At the Rx, the transmitted bits are recovered in the FD as in [24]. Note that, the negative clipping distortion of ACO-OFDM corresponding to the lower layer should be removed before correctly demodulating the higher layer in order to determine the optimal bit error rate (BER) performance. However, the optimal BER performance is achieved at the cost of further increased system complexity, hardware implementation and latency.

III. PROPOSED THO-OFDM SYSTEM

From Section II we can see that, the data capacity of LACO-OFDM increases with the layer number but at the cost of increased system complexity. Therefore, we propose a novel THO-OFDM scheme including double layers ACO-OFDM and single layer PAM-DMT signals to reach the η_{se} limit of LACO-OFDM with a much simpler transmitter (Tx) structure as shown in Fig. 1.

A. TRANSMITTER

The detailed Tx structure of the proposed THO-OFDM is shown in Fig. 2, where serial-to-parallel conversion, Hermitian symmetry and cyclic prefix (CP) insertion are omitted. The arbitrary binary bit sequence is first allocated to the 3-layer based on the modulation orders and IFFT points in each layer. Here, we define $X_{\text{ACO}}^{(1)}$, $X_{\text{ACO}}^{(2)}$ and $X_{\text{PAM}}^{(3)}$ as

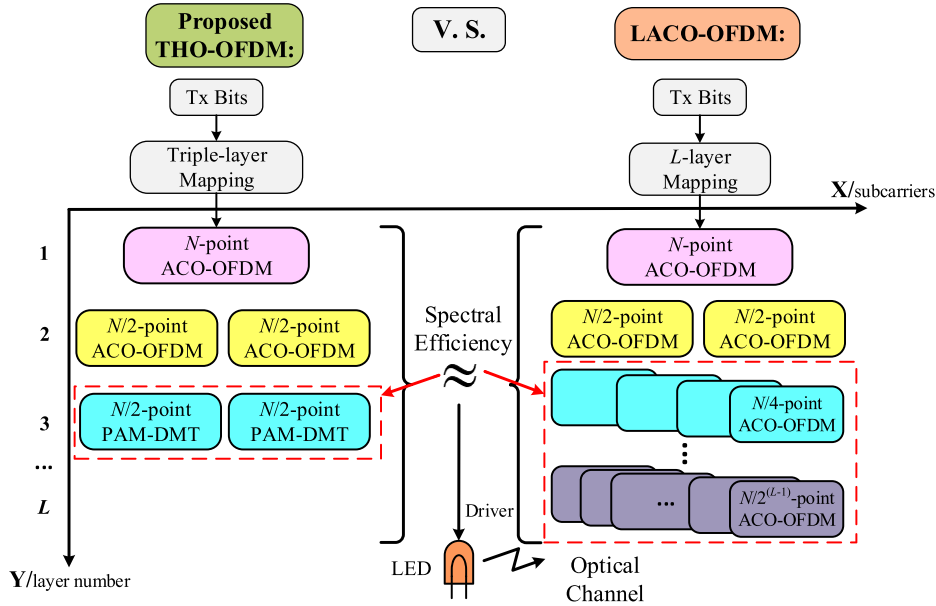


FIGURE 1. Comparisons of the proposed THO-OFDM and LACO-OFDM.

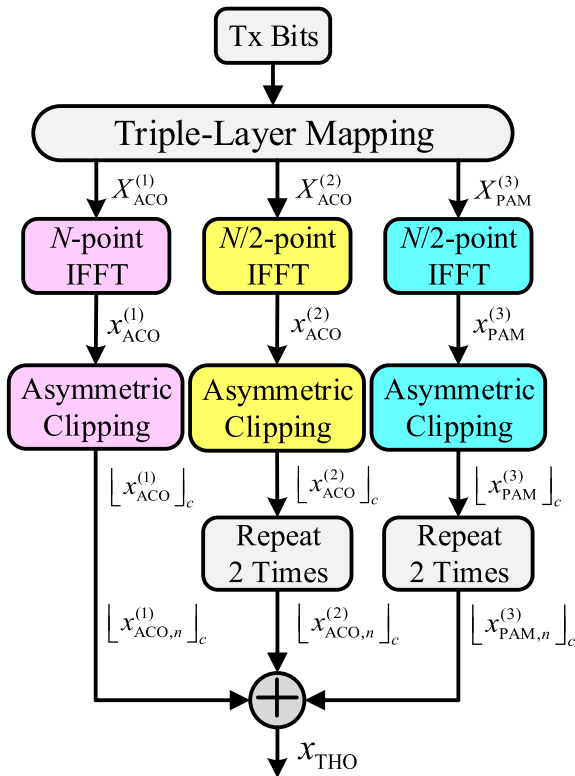


FIGURE 2. Block diagram of the proposed THO-OFDM Tx.

N -point QAM, $N/2$ -point QAM and $N/2$ -point PAM symbols corresponding to the 1st, 2nd and 3rd layers, respectively. $X_{ACO}^{(1)}$ is defined in (1), and $X_{ACO}^{(2)}$ and $X_{PAM}^{(3)}$ are given by:

$$X_{ACO}^{(2)} = [0, X_1, 0, X_3, \dots, X_{N/4-1}, 0, X_{N/4-1}^*, 0, \dots, X_3^*, 0, X_1^*], \quad (5)$$

$$X_{PAM}^{(3)} = j[0, 0, P_2, 0, P_4, \dots, P_{N/4-2}, 0, 0, 0, -P_{N/4-2}, 0, \dots, -P_4, 0, -P_2, 0], \quad (6)$$

where $j = \sqrt{-1}$ and $P_k (k = 2, 4, \dots, N/4 - 2)$ is the PAM symbols. Although the effective ACO-OFDM samples in the 2nd layer are half of the 1st layer in THO-OFDM, the length of effective PAM-DMT samples in the 3rd layer is the same as ACO-OFDM in the 2nd layer. By doing this, η_{se} of THO-OFDM is increased significantly compared with conventional LACO-OFDM. Note that, in THO-OFDM Hermitian symmetry is still required to ensure the anti-symmetric property for the first two layers of ACO-OFDM and the periodic property for the 3rd layer of PAM-DMT.

Following the IFFT operation at each layer, we will have the bipolar TD signals of $x_{ACO}^{(1)}$, $x_{ACO}^{(2)}$ and $x_{PAM}^{(3)}$. Negative clipping is applied to these signals to ensure all positive and real signals prior to applying the 2-time repeat operation to the 2nd and 3rd layers to compensating for the length difference. The constructed unipolar signals with the same length are defined as $[x_{ACO,n}^{(1)}]_c$, $[x_{ACO,n}^{(2)}]_c$ and $[x_{PAM,n}^{(3)}]_c$, where $n = 0, 1, \dots, N - 1$. Therefore, the TD signals in different layers have the different anti-symmetric and a periodic property, which can be concluded as below (7)–(9), as shown at the bottom of the next page.

Finally, the combined triple-layer unipolar signal is given as:

$$x_{THO} = [x_{ACO,n}^{(1)}]_c + [x_{ACO,n}^{(2)}]_c + [x_{PAM,n}^{(3)}]_c. \quad (10)$$

B. RECEIVER

In this part, we make full use of the special structure of THO-OFDM to represent the two different layered demodulation methods in the TD and FD, respectively.

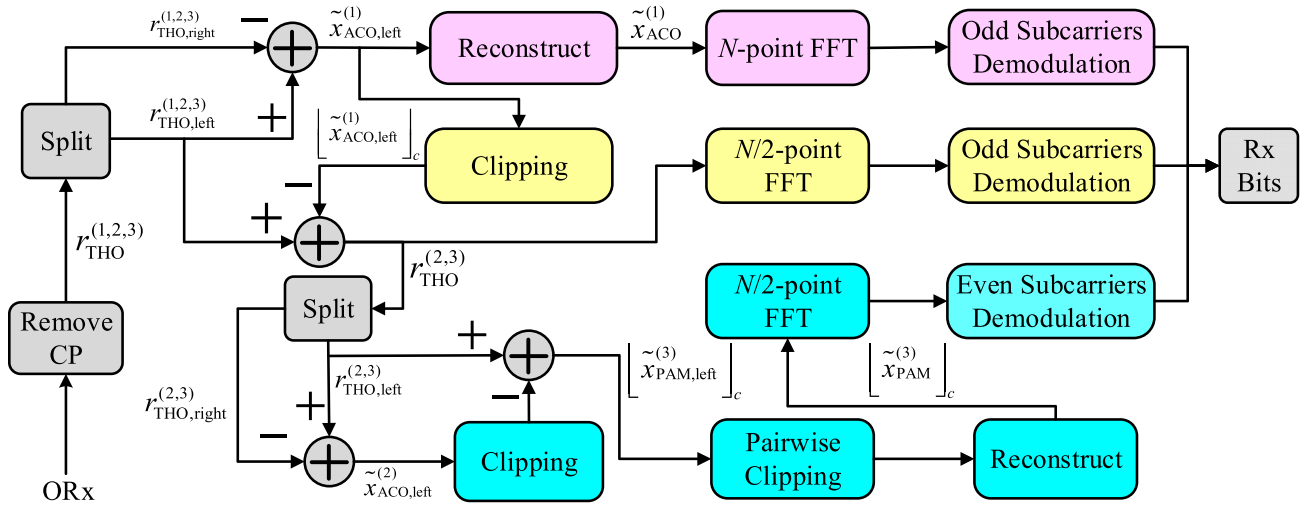


FIGURE 3. Block diagram of the proposed TD-based Rx for THO-OFDM.

The block diagram of the TD-based Rx for THO-OFDM is shown in Fig. 3. The received optical signal is first converted into an electrical signal using an optical Rx (ORx) prior to removing the CP. The noise due to optical and electrical parts as well as the ambient lights is modeled as an additive white Gaussian noise (AWGN) [27]–[31]. Thus, the received THO-OFDM signal is given as:

$$r_{\text{THO}}^{(1,2,3)} = R x_{\text{THO}} \otimes h(n) + w_n, \quad (11)$$

where R is the photodiode responsivity, $n = 0, 1, 2, \dots, N-1$, $h(n)$ is the channel impulse response (CIR), w_n denotes the discrete samples of AWGN and \otimes represents convolution operation [32]. To simplify the derivation processes, w_n is omitted in the following equations.

As for the TD-based Rx, following removal of the CP the signal $r_{\text{THO}}^{(1,2,3)}$ is split into two, which are given as:

$$r_{\text{THO},\text{left}}^{(1,2,3)} = \left[\tilde{x}_{\text{ACO},n}^{(1)} \right]_c + \left[\tilde{x}_{\text{ACO},n}^{(2)} \right]_c + \left[\tilde{x}_{\text{PAM},n}^{(3)} \right]_c, \quad (12)$$

$$r_{\text{THO},\text{right}}^{(1,2,3)} = \left[\tilde{x}_{\text{ACO},n+N/2}^{(1)} \right]_c + \left[\tilde{x}_{\text{ACO},n+N/2}^{(2)} \right]_c + \left[\tilde{x}_{\text{PAM},n+N/2}^{(3)} \right]_c, \quad (13)$$

where $n = 0, 1, \dots, N/2-1$. According to (7)-(9), estimated ACO-OFDM in the 1st layer is given by:

$$\begin{aligned} \tilde{x}_{\text{ACO},\text{left}}^{(1)} &= r_{\text{THO},\text{left}}^{(1,2,3)} - r_{\text{THO},\text{right}}^{(1,2,3)} \\ &= \left[\tilde{x}_{\text{ACO},n}^{(1)} \right]_c - \left[\tilde{x}_{\text{ACO},n+N/2}^{(1)} \right]_c, \end{aligned} \quad (14)$$

where $\tilde{x}_{\text{ACO},\text{left}}^{(1)}$ represents the left half part of the estimated 1st layer bipolar signal $x_{\text{ACO}}^{(1)}$. The N -point $x_{\text{ACO}}^{(1)}$ is reconstructed by employing the anti-symmetric property of $x_{\text{ACO}}^{(1)} = \left[\tilde{x}_{\text{ACO},\text{left}}^{(1)}, -\tilde{x}_{\text{ACO},\text{left}}^{(1)} \right]$. Following N -point FFT operation, the transmitted bits for the 1st layer is obtained by demodulation of QAM using the odd subcarriers in the FD.

As the superimposed N -point signal in the 2nd and 3rd layers in the TD contains half the repeated signal, the

$$\left[x_{\text{ACO},n}^{(1)} \right]_c = \left[-x_{\text{ACO},n+N/2}^{(1)} \right]_c, \quad n = 0, 1, \dots, N/2-1, \quad (7)$$

$$\begin{cases} \left[x_{\text{ACO},n}^{(2)} \right]_c = \left[x_{\text{ACO},n+N/2}^{(2)} \right]_c, & n = 0, 1, \dots, N/2-1 \\ \left[x_{\text{ACO},n}^{(2)} \right]_c = \left[-x_{\text{ACO},n+N/4}^{(2)} \right]_c, & n = 0, 1, \dots, N/4-1, \end{cases} \quad (8)$$

$$\begin{cases} \left[x_{\text{PAM},n}^{(3)} \right]_c = \left[x_{\text{PAM},n+N/2}^{(3)} \right]_c, & n = 0, 1, \dots, N/2-1 \\ \left[x_{\text{PAM},n}^{(3)} \right]_c = \left[x_{\text{PAM},n+N/4}^{(3)} \right]_c, & n = 0, 1, \dots, N/4-1 \\ \left[x_{\text{PAM},n}^{(3)} \right]_c = \left[-x_{\text{PAM},N/4-n}^{(3)} \right]_c, & n = 1, 2, \dots, N/8-1 \\ \left[x_{\text{PAM},0}^{(3)} \right]_c = \left[x_{\text{PAM},N/8}^{(3)} \right]_c = 0 \\ \left[x_{\text{PAM},N/4}^{(3)} \right]_c = \left[x_{\text{PAM},3N/8}^{(3)} \right]_c = 0. \end{cases} \quad (9)$$

$N/2$ -point effective signal can be utilized to realize the sub-optimal demodulation with reduced complexity. Note, the clipping signal of $\tilde{x}_{ACO, \text{left}}^{(1)}$ is removed from $r_{\text{THO, left}}^{(1,2,3)}$ to obtain the $N/2$ -point superimposed signal of the 2nd and 3rd layers, which can be expressed as:

$$r_{\text{THO}}^{(2,3)} = r_{\text{THO, left}}^{(1,2,3)} - \left[\tilde{x}_{ACO, \text{left}}^{(1)} \right]_c \quad (15)$$

Since clipping interference due to the 2nd and 3rd layers only effect the even subcarriers of $r_{\text{THO}}^{(2,3)}$, the ACO-OFDM signal of the 2nd layer is first recovered by means of the $N/2$ -point FFT operation. Prior to recovering PAM-DMT in the 3rd layer, the clipping interference from ACO-OFDM of the 2nd layer needs to be removed either in the frequency or time domain [30], [33]. Here, we have adopted the latter, which is simpler to implement and effective in reducing the clipping noise. First, $r_{\text{THO}}^{(2,3)}$ is split into left and right $N/4$ -point as $r_{\text{THO, left}}^{(2,3)}$, $r_{\text{THO, right}}^{(2,3)}$, respectively. The left half part of the 2nd layer bipolar ACO-OFDM signal is estimated as:

$$\begin{aligned} \tilde{x}_{ACO, \text{left}}^{(2)} &= r_{\text{THO, left}}^{(2,3)} - r_{\text{THO, right}}^{(2,3)} = \left[\tilde{x}_{ACO, n}^{(2)} \right]_c + \left[\tilde{x}_{PAM, n}^{(3)} \right]_c \\ &\quad - \left[\tilde{x}_{ACO, n+N/4}^{(2)} \right]_c - \left[\tilde{x}_{PAM, n+N/4}^{(3)} \right]_c \\ &= \left[\tilde{x}_{ACO, n}^{(2)} \right]_c - \left[\tilde{x}_{ACO, n+N/4}^{(2)} \right]_c, \end{aligned} \quad (16)$$

where $n = 0, 1, \dots, N/4 - 1$. Thus, the left half part of PAM-DMT in the 3rd layer can be estimated as:

$$\begin{aligned} \left[\tilde{x}_{PAM, n}^{(3)} \right]_c &= r_{\text{THO, left}}^{(2,3)} - \left[\tilde{x}_{ACO, \text{left}}^{(2)} \right]_c \\ &= \left[\tilde{x}_{ACO, n}^{(2)} \right]_c + \left[\tilde{x}_{PAM, n}^{(3)} \right]_c - \left[\tilde{x}_{ACO, \text{left}}^{(2)} \right]_c, \end{aligned} \quad (17)$$

According to (9), pairwise clipping can be utilized to reduce the noise by almost half and estimate the error for $\left[\tilde{x}_{PAM, n}^{(3)} \right]_c$ for further improvement of the BER performance of PAM-DMT [28], [34], which is expressed by:

$$\left[\tilde{x}_{PAM, \text{left}}^{(3)} \right]_c = \left[\tilde{x}_{PAM, n}^{(3)} \right]_c I \left\{ \left[\tilde{x}_{PAM, N/4-1-n}^{(3)} \right]_c \leq \left[\tilde{x}_{PAM, n}^{(3)} \right]_c \right\}, \quad (18)$$

where $n = 0, 1, \dots, N/8 - 1$ and $I(A)$ is an indicator function with $I(A) = 1$ if event A is true and $I(A) = 0$ otherwise. In addition, $\left[\tilde{x}_{PAM, 0}^{(3)} \right]_c$, $\left[\tilde{x}_{PAM, N/8}^{(3)} \right]_c$, $\left[\tilde{x}_{PAM, N/4}^{(3)} \right]_c$ and $\left[\tilde{x}_{PAM, 3N/8}^{(3)} \right]_c$ are also set to zero according to (9).

Next, $\left[\tilde{x}_{PAM}^{(3)} \right]_c$ can be reconstructed based on the periodic property. Finally, the transmitted bits for PAM-DMT in the 3rd layer can be demodulated from the imaginary parts of even subcarriers following the $N/2$ -point FFT operation.

As for the FD-based Rx, the subcarriers distribution for the signal and clipping distortion are shown in Fig. 4. The block diagram of the FD-based Rx for THO-OFDM is shown in Fig. 5. As shown in Fig. 4, there is no overlapping of clipping distortion with the data-carrying odd subcarriers for the Layer 1 with the index $K_1 = [1, 3, \dots, N-1]$. Therefore,

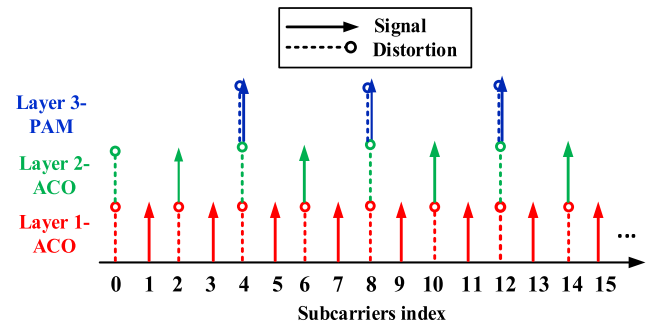


FIGURE 4. Block diagram of subcarriers mapping for the FD-based THO-OFDM.

the data can be estimated directly from K_1 using the standard demodulation of ACO-OFDM. For the Layer 1, following demodulation, the distortion level is estimated using the clipping noise regeneration process as in [24], [30]. Given that the data-carrying subcarriers of Layer 2 with the index $K_2 = [2, 6, \dots, N-2]$ is only affected by the clipping distortion of Layer 1, the Layer 2 can be demodulated by substituting the corresponding distortion components of the Layer 1. Unlike the FD structure of LACO-OFDM, for the Layer 3 of THO-OFDM the index of data-carrying subcarriers is $K_3 = [4, 8, \dots, N-4]$. The clipping distortion of PAM-DMT falls on the real part of corresponding even subcarriers in Layer 3, while the imaginary part of corresponding even subcarriers is independent of the PAM-DMT induced distortion. Therefore, the subcarriers of PAM can be extracted by substituting the corresponding distortion components of Layers 1 and 2.

IV. THEORY ANALYSIS OF THE THO-OFDM SYSTEM

A. SPECTRAL EFFICIENCY

The spectral efficiency of the proposed THO-OFDM is determined by the constellation combinations of N -point QAM, $N/2$ -point QAM and $N/2$ -point PAM symbols. The spectral efficiency for the standard ACO-OFDM and PAM-DMT are given as [26], [35]:

$$\eta_{ACO} = \frac{N \log_2 M_{ACO}}{4(N + N_{CP})} \text{ (bit/s/Hz)}, \quad (19)$$

$$\eta_{PAM} = \frac{(N-2) \log_2 M_{PAM}}{2(N + N_{CP})} \text{ (bit/s/Hz)}, \quad (20)$$

where M_{ACO} and M_{PAM} denote the constellation size of QAM and PAM symbols, respectively. Since only the even subcarriers of PAM-DMT are used to carry data information in the proposed scheme, the total spectral efficiency of the proposed THO-OFDM is given by:

$$\begin{aligned} \eta_{\text{THO}} &= \frac{1}{N + N_{CP}} \left(\sum_{l=1}^2 \frac{N \log_2 M_{ACO}^{(l)}}{2^{l+1}} + \frac{(N-2) \log_2 M_{PAM}^{(3)}}{8} \right) \\ &= \frac{\frac{N}{4} \log_2 M_{ACO}^{(1)} + \frac{N}{8} \log_2 M_{ACO}^{(2)} + \frac{N-2}{8} \log_2 M_{PAM}}{N + N_{CP}} \end{aligned} \quad (21)$$

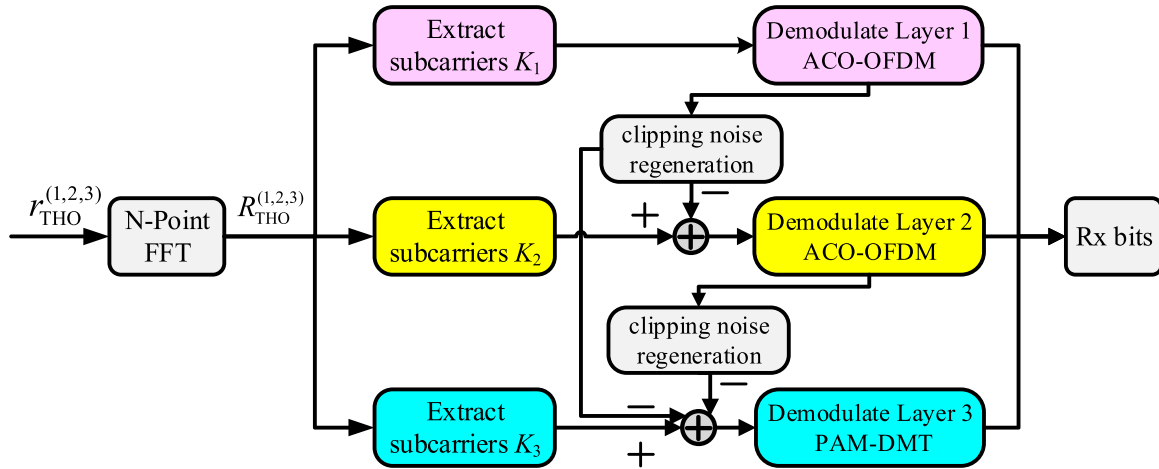


FIGURE 5. Block diagram of the proposed FD-based Rx for THO-OFDM.

where $M_{ACO}^{(l)}$ ($l = 1, 2$) and M_{PAM} are the constellation size of QAM and PAM symbols, respectively. For comparisons, the spectral efficiency of L -layer LACO-OFDM is given by:

$$\eta_{LACO} = \frac{1}{N + N_{CP}} \sum_{l=1}^L \frac{N}{2^{l+1}} \log_2 M_{ACO}^{(l)} \text{ (bit/s/Hz)}. \quad (22)$$

Based on (21)-(22), it can be concluded that $\eta_{LACO} \approx \eta_{THO}$ for $L \rightarrow \infty$, ignoring the effect of N_{CP} and for the same constellation size for LACO-OFDM and the proposed THO-OFDM. Therefore, THO-OFDM could theoretically achieve the spectral efficiency limit of LACO-OFDM with only three layers and the same constellation size.

B. COMPUTATION COMPLEXITY

The computation complexity in this work is defined as the number of complex multiplications in FFT/IFFT. In ACO-OFDM, the computation complexity of an N -point complex- and real-valued IFFT/FFT operations, respectively are defined as $O(N \log_2 N)$ and $O(N/2 \log_2 N)$ accordingly. Given that, in PAM-DMT the data is in the imaginary parts, the computation complexity of N -point IFFT/FFT operation is $O(N/2 \log_2 N)$ [26]. For comparisons, the computation complexities of the TD and FD-based Rxs for THO-OFDM and conventional LACO-OFDM [24] are both given in the following.

At the Tx, THO-OFDM requires one N -point and $N/2$ -point complex-valued IFFT and IFFT operations for $x_{ACO}^{(1)}$ and for $x_{ACO}^{(2)}$ and $x_{PAM}^{(3)}$, respectively. Therefore, the computation complexity of THO-OFDM can be expressed as:

$$\begin{aligned} O(\text{THO})_{Tx} &= O(N \log_2 N) + O(N/2 \log_2(N/2)) \\ &\quad + O(N/4 \log_2(N/2)) \\ &= O(N(\log_2 N + 3/4 \log_2(N/2))). \end{aligned} \quad (23)$$

Similarly, the computation complexity of L -layer conventional LACO-OFDM at the Tx can be given by (24):

$$\begin{aligned} O(\text{LACO})_{Tx} &= O\left(\sum_{l=1}^L (N/2^{l-1}) \log_2(N/2^{l-1})\right) \\ &= O\left(2N(1 - 2^{-L}) \log_2 N - 2N(1 - 2^{1-L})\right. \\ &\quad \left.+ (L - 1)N/2^{L-1}\right) \\ &= O(N \log_2 N + 3N/4 \log_2(N/2) - N \\ &\quad + N/4 \log_2(N/2) + 2^{1-L}N(L + 1 - \log_2 N)) \\ &= O(\text{THO})_{Tx} + F(N, L). \end{aligned} \quad (24)$$

Note, $F(N, L) = (N/4) \log_2(N/2) - N + 2^{1-L}N(L + 1 - \log_2 N)$, which satisfies $F(N, L) > 0$ if $L \geq 4$, $N > 32$ and $F(N, L) < 0$ if $2 \leq L < 4$.

At the Rx, the computation complexity of the proposed the TD and the FD based Rx of THO-OFDM are respectively given by (25) and (26):

$$\begin{aligned} O(\text{THO})_{Rx-TD} &= O(N/2 \log_2 N + N/4 \log_2(N/2) \\ &\quad + N/4 \log_2(N/2)) \\ &= O(N/2(\log_2 N + \log_2(N/2))) \\ &= O(N(\log_2 N - 1/2)). \end{aligned} \quad (25)$$

$$\begin{aligned} O(\text{THO})_{Rx-FD} &= O(N/2 \log_2 N + N \log_2 N + N/2 \log_2 N \\ &\quad + N/2 \log_2(N/2) + N/4 \log_2(N/2)) \\ &= O(N(2 \log_2 N + 3/4 \log_2(N/2))). \end{aligned} \quad (26)$$

Whereas, the computation complexity of the L -layer conventional LACO-OFDM at the Rx is given by (27):

$$\begin{aligned} O(\text{LACO})_{Rx} &= O\left(N \log_2(N) + 2 \sum_{l=1}^{L-1} (N/2^{l-1}) \log_2(N/2^{l-1})\right) \\ &> O(\text{THO})_{Rx-TD}. \end{aligned} \quad (27)$$

TABLE 1. Spectral efficiency (SE) and computation complexity (CC) comparisons.

	SE	CC		$CCRR_1$ (%)	$CCRR_2$ (%)	
		Tx	Rx			
THO-OFDM with TD	0.999	7680	4352	41.3	2.5	
THO-OFDM with FD			12288			
LACO-OFDM	$L=2$	0.750	6656	13824	52.8	21.6
	$L=3$	0.875	7552	17920	56.5	27.8
	$L=4$	0.938	7936	19712	57.9	30.1
	$L=5$	0.969	8096	20480	58.5	31.0
	$L=6$	0.984	8160	20800	58.7	31.4
	$L=7$	0.992	8184	20928	58.8	31.5
	$L=8$	0.996	8192	20976		

The total computation complexity of the proposed THO-OFDM and the conventional LACO-OFDM are given by (28):

$$\begin{cases} O(\text{THO})_{\text{TD}} = O(\text{THO})_{\text{Tx}} + O(\text{THO})_{\text{Rx-TD}} \\ O(\text{THO})_{\text{FD}} = O(\text{THO})_{\text{Tx}} + O(\text{THO})_{\text{Rx-FD}} \\ O(\text{LACO}) = O(\text{LACO})_{\text{Tx}} + O(\text{LACO})_{\text{Rx}} \end{cases} \quad (28)$$

Based on (25)-(26), we can conclude that the computation complexity of the TD-based Rx is lower compared with the FD-based Rx in THO-OFDM. In order to measure the computation complexity, here we define the computation complexity reduction ratio (CCRR) as in (29):

$$\begin{aligned} CCRR_1 &= 1 - \frac{O(\text{THO})_{\text{TD}}}{O(\text{LACO})} \\ CCRR_2 &= 1 - \frac{O(\text{THO})_{\text{FD}}}{O(\text{LACO})} \end{aligned} \quad (29)$$

For $N = 512$ and the maximum number of layer (i.e., $L_{\text{max}} = 8$) we have $CCRR_1 \approx 59\%$ and $CCRR_2 \approx 32\%$, which shows reduced computation complexity for the proposed THO-OFDM with TD and FD-based Rx compared with the conventional LACO-OFDM Rx as in [24]. Finally, η_{se} and computation complexity of the proposed THO-OFDM and conventional LACO-OFDM for range of layers are summarized in Table 1. Note, the effect of N_{CP} is not considered, N and $M_{\text{ACO}} = M_{\text{PAM}}$ are set to 512 and 4, respectively.

C. BER PERFORMANCE

The bit error probability for ACO-OFDM with M_{ACO} -ary square QAM and PAM-DMT with M_{PAM} -ary PAM are given

by [23], [36], [37]:

$$P_{b,\text{QAM}} \approx \frac{4(\sqrt{M_{\text{ACO}}} - 1)}{\sqrt{M_{\text{ACO}}} \log_2 M_{\text{ACO}}} Q\left(\sqrt{\frac{3 \log_2 M_{\text{ACO}} E_b}{M_{\text{ACO}} - 1 N_0}}\right), \quad (30)$$

$$P_{b,\text{PAM}} \approx \frac{2(M_{\text{PAM}} - 1)}{M_{\text{PAM}} \log_2 M_{\text{PAM}}} Q\left(\sqrt{\frac{6 \log_2 M_{\text{PAM}} E_b}{M_{\text{PAM}}^2 - 1 N_0}}\right), \quad (31)$$

where E_b is the bit energy, N_0 is the noise spectral density and $Q(\cdot)$ is the tail probability of the standard normal distribution given by $Q(\xi) = \frac{1}{\sqrt{2\pi}} \int_{\xi}^{\infty} \exp\left(-\frac{u^2}{2}\right) du$.

Based on (30)-(31), the average P_b for 3-layer THO-OFDM including N -point ACO-OFDM with $M_{\text{ACO}}^{(1)}$ -ary square QAM, $N/2$ -point ACO-OFDM with $M_{\text{ACO}}^{(2)}$ -ary square QAM and $N/2$ -point PAM-DMT with M_{PAM} -ary PAM is given by (32), as shown at the bottom of this page. Here, $P_{b,l}$ ($l = 1, 2, 3$) denotes the BER of the l^{th} layer of THO-OFDM. Since the BER performance of M^2 -ary square QAM is the same as M -ary PAM based on the above formulations, then we have $M_{\text{ACO}}^{(1)} = M_{\text{ACO}}^{(2)} = \sqrt{M_{\text{PAM}}} = M$ for a fair comparison for LACO-OFDM with the same η_{se} .

In order to ensure that different layers have similar BER performance at a given signal to noise ratio (SNR), the energy/bit for different layers should be kept the same. The theoretical analysis show that, the inter-layer BERs approximately satisfy $P_{b,1} = P_{b,2} = P_{b,3}$ in the FD demodulation provided $M_{\text{ACO}}^{(1)} = M_{\text{ACO}}^{(2)} = \sqrt{M_{\text{PAM}}} = M$. In the TD demodulation, see Fig. 3, however, the subtracting process following signal splitting will discard half of the noise component, which is totally different from the FD demodulation adopted in THO-OFDM or LACO-OFDM. Therefore, the single layer BER performance will degrade with the number of layers decreasing. Note that, BERs varies in the inter-layer, which can be exploited to improve the final BER, as was demonstrated in the TD iterative-based Rx of the HACO-OFDM and LACO-OFDM [28], [34].

V. NUMERICAL RESULTS

In this section, we outline the comprehensive BER, η_{se} , computation complexity and CCDF analysis obtained using Monte-Carlo simulations in the MATLAB R2016a. To simplify simulations, we consider the AWGN channel and the maximum number of subcarriers N of 512. Fig. 6 shows the BER as a function of SNR for the proposed THO-OFDM with TD/FD demodulation and conventional LACO-OFDM for 4-, 16-, and 64-QAM, 2-, 4-, and 8-PAM, and a range of η_{se} .

Since PAM only uses a one-dimension mapping to carry data bits compared with the two-dimension QAM constellations, the modulation orders in Fig. 6 should satisfy $M_{\text{ACO}} = \sqrt{M_{\text{PAM}}}$ for a fair comparison. From Fig. 6, we can see that,

$$P_{b,\text{THO}} = \frac{\frac{N}{4} \log_2 M_{\text{ACO}}^{(1)} P_{b,1} + \frac{N}{8} \log_2 M_{\text{ACO}}^{(2)} P_{b,2} + \left(\frac{N}{8} - 1\right) \log_2 M_{\text{PAM}} P_{b,3}}{\frac{N}{4} \log_2 M_{\text{ACO}}^{(1)} + \frac{N}{8} \log_2 M_{\text{ACO}}^{(2)} + \left(\frac{N}{8} - 1\right) \log_2 M_{\text{PAM}}}, \quad (32)$$

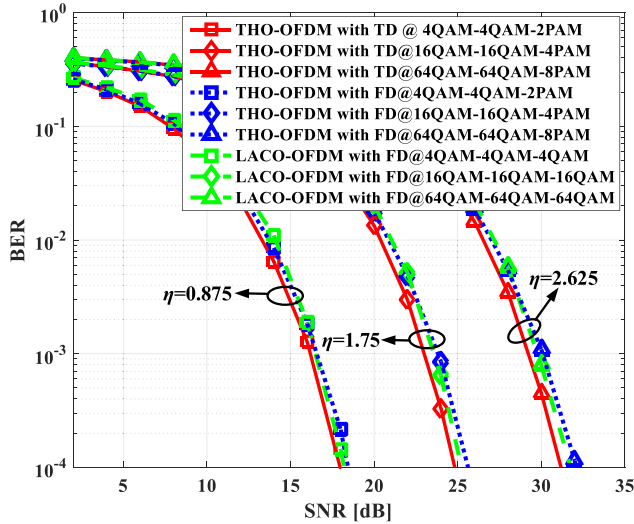


FIGURE 6. BER performance against SNR for the proposed THO-OFDM with TD and FD demodulation and conventional LACO-OFDM for different η_{se} (bit/s/Hz).

the proposed THO-OFDM with two demodulation methods can achieve the same η_{se} as LACO-OFDM with 3-layer. More specifically, η_{se} of 0.875 bit/s/Hz, 1.75 bit/s/Hz and 2.625 bit/s/Hz provided $M_{ACO} = \sqrt{M_{PAM}}$, where $M_{ACO} = 4, 16, 64$. Moreover, at a BER of 10^{-4} THO-OFDM with TD demodulation offer the SNR gains of 0.6, 0.8, and 1.0 dB compared with FD demodulation for $M_{ACO} = 4, 16$ and 64 , which marginally better than LACO-OFDM with FD demodulation.

To better illustrate the inter-layer BERs comparison of THO-OFDM with two demodulation methods, the BER plots for 1-3 layers in THO-OFDM with two demodulation methods for 4-QAM, 4QAM and 2PAM are depicted in Fig. 7. Note, the BER plots are obtained for layer-by-layer from low to high. As shown in Fig. 7, the inter-layer BERs plots for FD demodulation approximately approach at a given SNR value while the inter-layer BERs of TD demodulation turn better with the layer number increases. This is consistent with the theoretical analysis for the BER given in Section IV.

The detailed comparisons of η_{se} and computation complexity for the proposed THO-OFDM with two demodulation methods and the conventional LACO-OFDM are drawn in Fig. 8 for $M_{ACO} = M_{PAM} = 4$. Obviously, the proposed THO-OFDM with TD or FD achieve the spectral efficiency limit of LACO-OFDM with the computation complexity reduced significantly, which is also consistent with the previous analysis. E.g., for $L = 3$, we can further verify the advantages of the proposed THO-OFDM in terms of η_{se} of 0.124 bit/s/Hz and $CCRR_1 \approx 53\%$ in TD and $CCRR_2 \approx 22\%$ in FD compared with the conventional LACO-OFDM. Meanwhile, $\sim 40\%$ computation complexity reduction is achieved in TD demodulation compared with FD demodulation for THO-OFDM.

As the transfer characteristic of the commercial LEDs is nonlinear, the PAPR becomes another key factor to evaluate

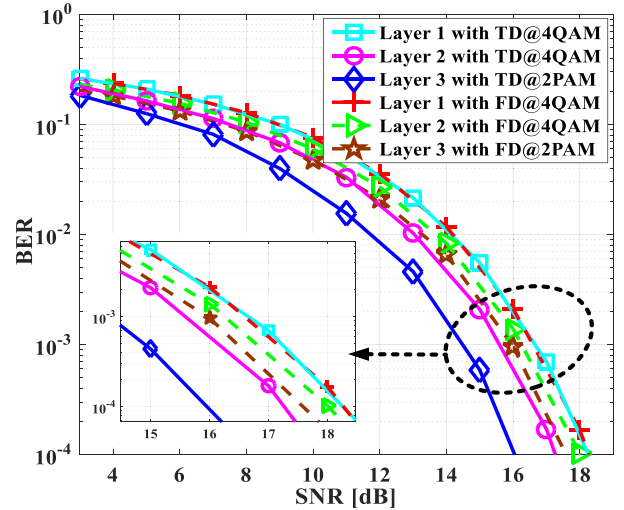


FIGURE 7. Inter-layer BER as function of SNR for the proposed THO-OFDM with the TD and FD demodulation for 4QAM, 4QAM and 2PAM.

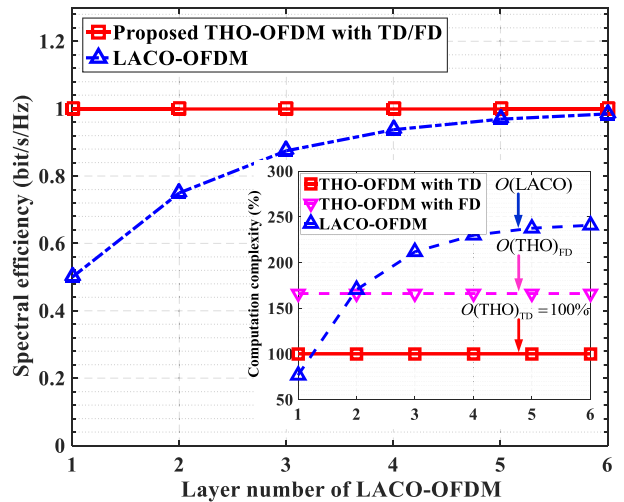


FIGURE 8. Comparisons of η_{se} and computation complexity of the proposed THO-OFDM with TD, FD and LACO-OFDM.

the performance of the optical OFDM [29], [38]–[40]. The PAPR of discrete optical OFDM signal can be generally defined as the ratio of the maximum power to the average power, which is given by:

$$PAPR = 10 \log_{10} \frac{\max |x(n)|^2}{E[|x(n)|^2]} \text{ (dB)}, \quad (33)$$

where $E[\cdot]$ denotes the statistical expectation. The complementary cumulative distribution function (CCDF) is further employed to illustrate the PAPR performance comparisons between the proposed THO-OFDM and the conventional LACO-OFDM. It denotes the probability that, PAPR of an optical OFDM signal exceeds a certain threshold $PAPR_0$ as given by:

$$CCDF = Pr(PAPR > PAPR_0). \quad (34)$$

Fig. 9 shows the CCDF against the threshold $PAPR_0$ for the proposed THO-OFDM and LACO-OFDM for a range

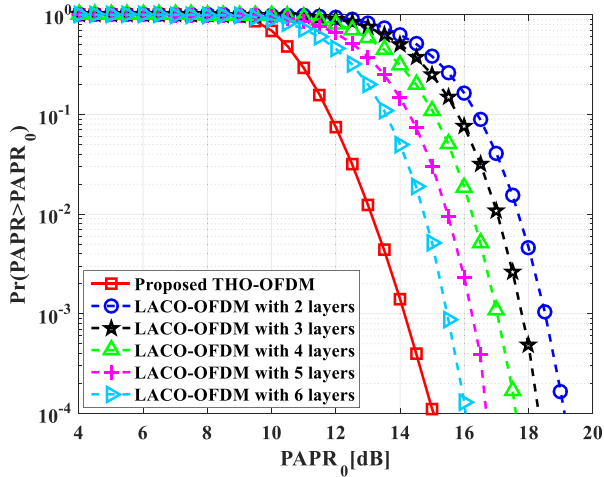


FIGURE 9. PAPR analysis for the proposed THO-OFDM and conventional LACO-OFDM with different layers under $M_{ACO} = M_{PAM} = 4$.

of layers. It is shown that, at the CCDF of 10^{-4} , the PAPR requirements are > 19 , > 18 , ~ 17.5 , ~ 17 and ~ 16 dB for LACO-OFDM for $L = 2, 3, 4, 5$ and 6 , respectively compared with 15 dB for the proposed THO-OFDM. It is worth noting that, for $L \geq 6$ there is a tendency that, the PAPR requirement for the proposed THO-OFDM is still lower than LACO-OFDM. For LACO-OFDM with more layers, fewer zeros would be found in the TD signal, due to the superposition of more layers. Meanwhile, the average power of the signal increases faster than the peak power as more layers are utilized [29]. Therefore, the LACO-OFDM signal with more layers tends to exhibit lower PAPR, which can also be verified from Fig. 9. However, at the CCDF of 10^{-4} , the proposed scheme offers lower $PAPR_0$ by about 3 dB compared with LACO-OFDM for the same number of layers and the modulation format.

VI. CONCLUSION

In this paper, a spectrum-efficient triple-layer hybrid optical orthogonal frequency division multiplexing was presented and studied. We showed that, the proposed THO-OFDM reached the spectral efficiency limit of the classical LACO-OFDM with only three layers. In addition, theoretical analysis results demonstrated that, THO-OFDM with the TD-based Rx did attain reduced computation complexity by 40% compared with the conventional successive interference cancellation (SIC) demodulation scheme employed in the frequency domain with a marginally improved BER. In addition, CCDF simulation results demonstrated that, a 3 dB PAPR improvement for THO-OFDM compared with the classical LACO-OFDM for the same number of layers, thus demonstrating its potential applications in IM/DD based optical wireless communications.

ACKNOWLEDGMENT

The authors would like to thank Dr. Qi Wang graduated from Tsinghua University for the fruitful discussions on LACO-OFDM and generously helps on simulation codes.

REFERENCES

- [1] Z. Ghassemlooy, S. Arnon, M. Uysal, Z. Xu, and J. Cheng, "Emerging optical wireless communications—advances and challenges," *IEEE J. Sel. Areas Commun.*, vol. 33, no. 9, pp. 1738–1749, Sep. 2015.
- [2] Z. Ghassemlooy, W. O. Popoola, and S. Rajbhandari, *Optical Wireless Communications—System and Channel Modelling With MATLAB*, 2nd ed. Boca Raton, FL, USA: CRC Publisher, Aug. 2019.
- [3] N. Chi, H. Haas, M. Kavehrad, T. D. Little, and X.-L. Huang, "Visible light communications: Demand factors, benefits and opportunities," *IEEE Wireless Commun.*, vol. 22, no. 2, pp. 5–7, Apr. 2015.
- [4] R. Zhang, H. Claussen, H. Haas, and L. Hanzo, "Energy efficient visible light communications relying on amorphous cells," *IEEE J. Sel. Areas Commun.*, vol. 34, no. 4, pp. 894–906, Apr. 2016.
- [5] H. Haas, L. Yin, Y. Wang, and C. Chen, "What is LiFi?" *J. Lightw. Technol.*, vol. 34, no. 6, pp. 1533–1544, Mar. 15, 2016.
- [6] Y.-C. Chuang, Z.-Q. Li, C.-W. Hsu, Y. Liu, and C.-W. Chow, "Visible light communication and positioning using positioning cells and machine learning algorithms," *Opt. Express*, vol. 27, no. 11, p. 16377, May 2019.
- [7] B. Lin, X. Tang, Z. Ghassemlooy, C. Lin, and Y. Li, "Experimental demonstration of an indoor VLC positioning system based on OFDMA," *IEEE Photon. J.*, vol. 9, no. 2, pp. 1–9, Apr. 2017.
- [8] Z. Zhang, T. Zhang, J. Zhou, Y. Lu, and Y. Qiao, "Thresholding scheme based on boundary pixels of stripes for visible light communication with mobile-phone camera," *IEEE Access*, vol. 6, pp. 53053–53061, 2018.
- [9] Y. Wang, X. Huang, L. Tao, and N. Chi, "1.8-Gb/s WDM visible light communication over 50-meter outdoor free space transmission employing CAP modulation and receiver diversity technology," in *Proc. Opt. Fiber Commun. Conf. Exhib. (OFC)*, Mar. 2015, pp. 1–3.
- [10] J. Wang, C. Lu, S. Li, and Z. Xu, "100 m/500 Mbps underwater optical wireless communication using an NRZ-OOK modulated 520 nm laser diode," *Opt. Express*, vol. 27, no. 9, pp. 12171–12181, Apr. 2019.
- [11] Y. Zhou, X. Zhu, F. Hu, J. Shi, F. Wang, P. Zou, J. Liu, F. Jiang, and N. Chi, "Common-anode LED on a Si substrate for beyond 15 Gbit/s underwater visible light communication," *Photon. Res.*, vol. 7, no. 9, pp. 1019–1029, Sep. 2019.
- [12] H. Le Minh, D. O'brien, G. Faulkner, L. Zeng, K. Lee, D. Jung, Y. Oh, and E. Tae Won, "100-Mb/s NRZ visible light communications using a postequalized white LED," *IEEE Photon. Technol. Lett.*, vol. 21, no. 15, pp. 1063–1065, Aug. 1, 2009.
- [13] M.-A. Khalighi, S. Long, S. Bourennane, and Z. Ghassemlooy, "PAM- and CAP-based transmission schemes for visible-light communications," *IEEE Access*, vol. 5, pp. 27002–27013, 2017.
- [14] X. Huang, Z. Wang, J. Shi, Y. Wang, and N. Chi, "16 Gbit/s phosphorescent white LED based VLC transmission using a cascaded pre-equalization circuit and a differential outputs PIN receiver," *Opt. Express*, vol. 23, no. 17, pp. 22034–22042, Aug. 2015.
- [15] Y. Wang and N. Chi, "Investigation of advanced pre- and post-equalization schemes in high-order CAP modulation based high-speed indoor VLC transmission system," *Proc. SPIE*, vol. 10019, pp. 100190C-1–100190C-9, Oct. 2016.
- [16] Y. Wang, L. Tao, X. Huang, J. Shi, and N. Chi, "Enhanced performance of a high-speed WDM CAP64 VLC system employing Volterra series-based nonlinear equalizer," *IEEE Photon. J.*, vol. 7, no. 3, Jun. 2015, Art. no. 7901907.
- [17] K. O. Akande, P. A. Haigh, and W. O. Popoola, "On the implementation of carrierless amplitude and phase modulation in visible light communication," *IEEE Access*, vol. 6, pp. 60532–60546, 2018.
- [18] J. Armstrong, "OFDM for optical communications," *J. Lightw. Technol.*, vol. 27, no. 3, pp. 189–204, Feb. 1, 2009.
- [19] S. Lee, S. Randel, F. Breyer, and A. Koonen, "PAM-DMT for intensity-modulated and direct-detection optical communication systems," *IEEE Photon. Technol. Lett.*, vol. 21, no. 23, pp. 1749–1751, Dec. 1, 2009.
- [20] S. D. Dissanayake and J. Armstrong, "Comparison of ACO-OFDM, DCO-OFDM and ADO-OFDM in IM/DD systems," *J. Lightw. Technol.*, vol. 31, no. 7, pp. 1063–1072, Apr. 1, 2013.
- [21] T. Zhang, Y. Zou, J. Sun, and S. Qiao, "Design of PAM-DMT-based hybrid optical OFDM for visible light communications," *IEEE Wireless Commun. Lett.*, vol. 8, no. 1, pp. 265–268, Feb. 2019.
- [22] L. Chen, B. Krongold, and J. Evans, "Successive decoding of anti-periodic OFDM signals in IM/DD optical channel," in *Proc. IEEE Int. Conf. Commun.*, May 2010.
- [23] L. Chen, B. Krongold, and J. Evans, "Performance analysis for optical OFDM transmission in short-range IM/DD systems," *J. Lightw. Technol.*, vol. 30, no. 7, pp. 974–983, Apr. 1, 2012.

- [24] Q. Wang, C. Qian, X. Guo, Z. Wang, D. G. Cunningham, and I. H. White, "Layered ACO-OFDM for intensity-modulated direct-detection optical wireless transmission," *Opt. Express*, vol. 23, no. 9, pp. 12382–12393, May 2015.
- [25] M. S. Islam, D. Tsonev, and H. Haas, "Spectrally enhanced PAM-DMT for IM/DD optical wireless communications," in *Proc. IEEE 26th Annu. Int. Symp. Pers., Indoor, Mobile Radio Commun. (PIMRC)*, Aug. 2015, pp. 877–882.
- [26] M. S. Islam and H. Haas, "Augmenting the spectral efficiency of enhanced PAM-DMT-based optical wireless communications," *Opt. Express*, vol. 24, no. 11, pp. 11932–11949, May 2016.
- [27] T. Zhang, Z. Ghassemlooy, S. Rajbhandari, W. O. Popoola, and S. Guo, "OFDM-PWM scheme for visible light communications," *Opt. Commun.*, vol. 385, pp. 213–218, Feb. 2017.
- [28] Q. Wang, Z. Wang, and L. Dai, "Iterative receiver for hybrid asymmetrically clipped optical OFDM," *J. Lightw. Technol.*, vol. 32, no. 22, pp. 4471–4477, Nov. 15, 2014.
- [29] X. Zhang, Q. Wang, R. Zhang, S. Chen, and L. Hanzo, "Performance analysis of layered ACO-OFDM," *IEEE Access*, vol. 5, pp. 18366–18381, 2017.
- [30] B. Ranjha and M. Kavehrad, "Hybrid asymmetrically clipped OFDM-based IM/DD optical wireless system," *J. Opt. Commun. Netw.*, vol. 6, no. 4, p. 387, Apr. 2014.
- [31] R. Zhang and L. Hanzo, "Multi-layer modulation for intensity-modulated direct-detection optical OFDM," *J. Opt. Commun. Netw.*, vol. 5, no. 12, p. 1402, Dec. 2013.
- [32] Z. Ghassemlooy, L. N. Alves, S. Zvanovec, and M. A. Khalighi, *Visible Light Communications: Theory and Applications*. Boca Raton, FL, USA: CRC Press, 2017, pp. 76–77.
- [33] T. Wang, Y. Hou, and M. Ma, "A novel receiver design for HACO-OFDM by time-domain clipping noise elimination," *IEEE Commun. Lett.*, vol. 22, no. 9, pp. 1862–1865, Sep. 2018.
- [34] Q. Wang, Z. Wang, X. Guo, and L. Dai, "Improved receiver design for layered ACO-OFDM in optical wireless communications," *IEEE Photon. Technol. Lett.*, vol. 28, no. 3, pp. 319–322, Feb. 1, 2016.
- [35] M. S. Islam, D. Tsonev, and H. Haas, "On the superposition modulation for OFDM-based optical wireless communication," in *Proc. IEEE Global Conf. Signal Inf. Process. (GlobalSIP)*, Dec. 2015, pp. 1022–1026.
- [36] K. Cho and D. Yoon, "On the general BER expression of one- and two-dimensional amplitude modulations," *IEEE Trans. Commun.*, vol. 50, no. 7, pp. 1074–1080, Jul. 2002.
- [37] J. Li, X.-D. Zhang, Q. Gao, Y. Luo, and D. Gu, "Exact BEP analysis for coherent M-ary PAM and QAM over AWGN and Rayleigh fading channels," in *Proc. VTC Spring IEEE Veh. Technol. Conf.*, May 2008, pp. 390–394.
- [38] J. Wang, Y. Xu, X. Ling, R. Zhang, Z. Ding, and C. Zhao, "PAPR analysis for OFDM visible light communication," *Opt. Express*, vol. 24, no. 24, pp. 27457–27474, Nov. 2016.
- [39] T. Zhang, Y. Zou, J. Sun, and S. Qiao, "Improved companding transform for PAPR reduction in ACO-OFDM-based VLC systems," *IEEE Commun. Lett.*, vol. 22, no. 6, pp. 1180–1183, Jun. 2018.
- [40] W. O. Popoola, Z. Ghassemlooy, and B. G. Stewart, "Pilot-assisted PAPR reduction technique for optical OFDM communication systems," *J. Lightw. Technol.*, vol. 32, no. 7, pp. 1374–1382, Apr. 1, 2014.



HAN JI received the B.Eng. degree from the Engineering Institute, Huaqiao University, Quanzhou, China, in 2014. He is currently pursuing the M.Eng. degree in electronics and communication engineering with the School of Physics, Northeast Normal University, Changchun, China. Since 2019, he has been the Master of Trainee with the Quanzhou Institute of Equipment Manufacturing, Haixi Institutes, Chinese Academy of Sciences, Quanzhou. His current research interests include optical OFDM modulation technique and theory optimization for visible light communications and optical networks.



ZABIH GHASSEMLOOY (Senior Member, IEEE) received the B.Sc. (Hons.) degree in electrical and electronics engineering from Manchester Metropolitan University, U.K., in 1981, and the M.Sc. and Ph.D. degrees from the University of Manchester, U.K., in 1984 and 1987, respectively. He is currently pursuing the C.Eng. degree. From 1987 to 1988, he was a Postdoctoral Research Fellow with the City, University of London, U.K. In 1988, he joined Sheffield Hallam University as a Lecturer, where he became a Professor, in 1997. In 2004, he joined the University of Northumbria, Newcastle upon Tyne, as the Associate Dean (AD) of research with the School of Engineering. From 2012 to 2014, he was the AD of the Research and Innovation, Faculty of Engineering and Environment, where he is currently the Head of the Optical Communications Research Group. He was a Research Fellow and a Distinguished Professor with the Chinese Academy of Science, Quanzhou, China, in 2015 and 2016, respectively. He was a Visiting Professor with University Tun Hussein Onn Malaysia, from 2013 to 2017, and Huaqiao University, China, from 2017 to 2018. He has published over 850 articles (330 journals and eight books), 97 keynote/invited talks, and supervised 65 Ph.D. students. He is also a coauthor of a CRC book on *Optical Wireless Communications—Systems and Channel Modeling with Matlab* (First Edition 2012 and Second Edition 2019). His research interests include optical wireless communications, free space optics, visible light communications, radio over fibre-free space optics, and sensor networks with project funding from EU, U.K. Research Council and industry. He is also a Fellow of IET and OSA. He was the Vice-Chair of EU Cost Action IC1101, from 2011 to 2016. In 2001, he was awarded the Tan Chin Tuan Fellowship in engineering from Nanyang Technological University, Singapore. He has been the Vice-Chair of the OSA Technical Group of Optics in Digital Systems, since 2018. He is also the Founder and the Chair of the IEEE/IET International Symposium on Communications Systems, Networks and DSP and West Asian Colloquium on Optical Wireless Communications. He has been the Co-Founder of a number of international events, including Workshop on Optical Wireless Communications in ICC, since 2015. He has been the Chair of the IEEE Student Branch at Northumbria University, Newcastle upon Tyne, since 2019. From 2004 to 2006, he was the IEEE U.K./IR Communications Chapter Secretary, the Vice-Chairman, from 2006 to 2008, the Chairman, from 2008 to 2011, and the Chairman of the IET Northumbria Network from, October 2011 to 2015. He was a Co-Editor of four books, including the Springer book on *Optical Wireless Communications—An Emerging Technology* (2016), the CRC book on *Visible Light Communications: Theory and Applications* (2017), the IGI Global book on *Intelligent Systems for Optical Networks Design: Advancing Techniques* (2013), and the IET book on *Analogue Optical Fibre Communications* and the *IEE Telecommunication series 32* (1995). He is also the Chief Editor of the *British Journal of Applied Science and Technology* and the *International Journal of Optics and Applications*. He is also the Associate Editor of a number of international journals and the Co-Guest Editor of a number of special issues.



TIAN ZHANG received the B.Sc. and the M.Sc. degrees in electronic science and technology from the Changchun University of Science and Technology, Changchun, China, in 2010 and 2013, respectively, and the Ph.D. degree in electronic circuit and systems from the State Key Laboratory on Integrated Optoelectronics, College of Electronic Science and Engineering, Jilin University, Changchun, in 2017. From 2015 to 2016, he was a visiting Ph.D. Student with the Optical Communication Research Group (OCRG), University of Northumbria, Newcastle upon Tyne, U.K. Since 2017, he has been a Lecturer with the School of Physics, Northeast Normal University, Changchun. He has authored over ten IEEE, OSA, IET, Elsevier journals, and six conference papers. His current research interests include OFDM modulation and digital signal processing for optical and wireless communications.



XUAN TANG received the B.Eng. (Hons.) degree in electric and communication engineering from Northumbria University, Newcastle upon Tyne, U.K, in 2008, and the Ph.D. degree in free-space optical communications with the Optical Communications Research Laboratory (OCRG), Northumbria University, in 2012. She worked as a Research/Teaching Assistant with the Electrical Engineering Department, Northumbria University, from 2008 to 2009. From 2012 to 2014, she was a

Postdoctoral Research Fellow with the Optical Wireless Information Systems Laboratory, Department of Electronic Engineering, Tsinghua University, Beijing, China. She is currently the Project Leader and a Researcher with the Quanzhou Institute of Equipment Manufacturing, Haixi Institutes, Chinese Academy of Sciences, Quanzhou, China. She has obtained and participated more than 20 projects. She has published over 100 articles of which half are SCI indexed. Her research interests are in the areas of optical wireless communication systems including high-speed infrared/ultraviolet laser communications, visible light communications and optical fiber systems, and radio frequency communication technologies.



BANGJIANG LIN received the B.Sc. and the Ph.D. degrees from the Electronics Engineering Department, Peking University, Beijing, China, in 2010 and 2015, respectively. He joined with the Quanzhou Institute of Equipment Manufacturing, Haixi Institutes, Chinese Academy of Sciences, in 2015, as a Lecturer, where he became an Associate Professor, in 2017. He has published more than 100 articles of which half are SCI indexed. His current research interests include passive optical

networks and visible light communications.



SHUANG QIAO received the B.Sc. degree from the Department of Physics, Jilin Normal University, in 1985, the M.Sc. degree from the Department of Physics, Northeast Normal University, Changchun, China, in 1990, and the Ph.D. degree from the Changchun Institute of Optics, Fine Mechanics and Physics, Chinese Academy of Sciences, Changchun, in 2004. From 1998 to 2000, he was a Foreign Postgraduate with the Faculty of Science, Osaka Kyoiku University, Osaka, Japan.

From 2004 to 2006, he held a postdoctoral position at the Changchun Institute of Optics, Fine Mechanics and Physics, Chinese Academy of Sciences. Since 2000, he has been a Professor with the School of Physics, Northeast Normal University. His research interests include the fields of nuclear imaging and nuclear signal processing, nuclear tube systems, ghost imaging technology, and digital signal processing for wireless communication.

• • •